Journal of Magnetic Resonance **147,** 116–120 (2000)
doi:10.1006/jmre.2000.2168, available online at http://www.idealibrary.com on IDEAL®

Rapid Acquisition Transverse Relaxometric Imaging

Mark D. Does and John C. Gore*

*Department of Diagnostic Radiology and *Applied Physics, Yale University School of Medicine, New Haven, Connecticut 06520*

Received May 12, 2000; revised July 12, 2000

Segmented echo-planar acquisitions have been incorporated into a multiecho imaging sequence to produce a MRI method for rapid transverse relaxometry. The method is demonstrated on gel phantoms and rat brain and found to produce unbiased estimates of T_2. Gradient performance can be a limiting factor for the implementation of this technique and there is a cost in signal-to-noise ratio resulting from the higher bandwidth required, as is typical for echo-planar acquisitions.

Key Words: **MRI; T_2; EPI; fast imaging; relaxometry.**

INTRODUCTION

Accurate measurements of the transverse relaxation times (T_2) of NMR signals are of broad interest for numerous applications of NMR, including the study of microstructure. When the microstructure of a sample is compartmentalized on a physical scale which is much smaller than the spatial resolution in an image, it may still be possible to identify subvoxel compartments through their unique NMR signal characteristics. In this manner, multiexponential T_2 (MET_2) characteristics of tissue have been studied for some time. Multiecho imaging methods have been developed (*1*) and implemented with some success to study MET_2 characteristics of tissues *in vivo* (*2–4*). However, because such MET_2 imaging methods use conventional *k*-space acquisitions (one line per repetition time (TR)-interval) and generally require high resolution (to avoid partial volume artifacts) and long repetition times (to avoid bias from multiple longitudinal relaxation time (T_1) components), scan times are long. Furthermore, in addition to measuring MET_2 characteristics of a sample there is growing interest in integrated studies of other NMR parameters (e.g., magnetisation transfer, T_1, diffusion) with MET_2 characteristics (*5–11*). These studies may be useful in elucidating physical characteristics of subvoxel water compartments; however, due to long scan times, such investigations are limited in extent when implemented with conventional multiecho imaging methods.

Although significant efforts have been made to establish accurate imaging methods for MET_2 quantification, little has been done to reduce acquisition times of these techniques. Previous publications on rapid T_2 imaging have been aimed toward the generation of single-component T_2 maps (*12, 13*), but these techniques are not generally useful for relaxometry where MET_2 relaxation is anticipated. Yablonskiy recently proposed a method of extracting T_2 relaxation from T_2^* decay curves in postprocessing, but it remains to be seen whether this approach will be practical for quantifying MET_2 (*14*). There are a few published accounts of quantifying multiexponential relaxation *in vivo* using single-voxel techniques, which provide both rapid acquisition times and high signal-to-noise ratios (SNR) (*15–17*). However, these methods are not well suited to extracting data from difficult-to-segment regions of interest (ROI) and can only acquire data from one ROI at a time.

In general, one of two approaches can be taken to reduce MRI acquisition times: (i) reduce TR delay between acquisition of lines of *k*-space or (ii) acquire multiple *k*-space lines during each TR. The former approach is simple and effective for many cases, but not so for MET_2 quantification, because reduced TR with 90° excitation pulses will bias the contribution of different water compartments with different T_1s. This effect can be mitigated by using smaller tip-angle excitation pulses, but the series of hard refocusing pulses in a multiecho imaging sequence cannot be assumed to have no net effect on the remaining longitudinal magnetization.

A more promising approach for faster multiecho imaging involves acquiring multiple lines of *k*-space per TR interval. In the limit of full *k*-space acquisition per spin echo, this extends to a multiecho echo-planar imaging (EPI) scheme, such as that presented recently (*18*), although this case limits resolution and interecho spacing. In this paper the general case is considered in which a number, N_{GE}, of gradient echoes are collected for each spin echo of a multiecho imaging sequence. We designate this approach *r*apid *a*cquisition *t*ransverse r*e*laxometric (RATE) imaging and examine its strengths and limitations.

PULSE SEQUENCE

An example of a RATE pulse sequence is shown in Fig. 1 and is composed of the following distinguishing characteristics. The RF train is that of a CPMG sequence with a slice-selective excitation pulse and composite refocusing pulses for improved insensitivity to B_0 and B_1 inhomogeneity. (If multislice acquisition is desired, these refocusing pulses can be made slice-selective at the cost of reduced refocusing efficiency, which will increase apparent R_2s.) Surrounding the refocusing pulses are slice-direction spoiler gradients, which

1090-7807/00 $35.00

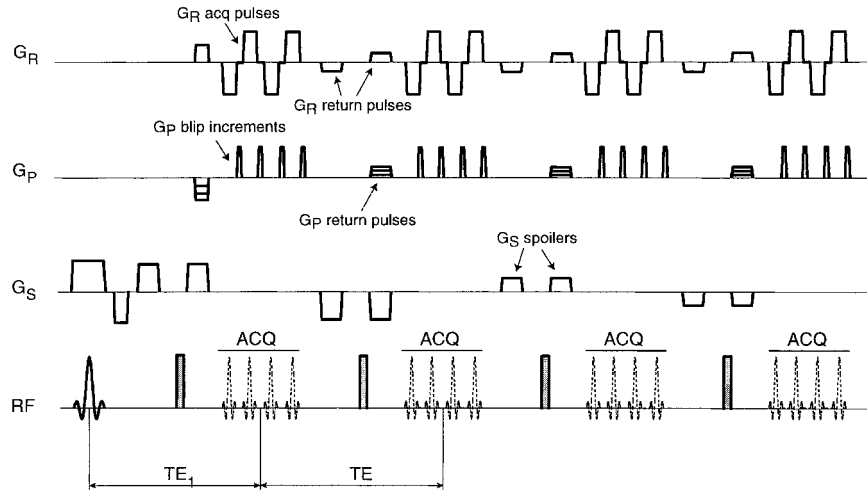

FIG. 1. An example of a RATE pulse sequence which collects four echo images (NE) with a $N_{GE} = 4$. The stepped phase gradients following the second through fourth RF refocusing pulses and the small read gradients surrounding these same pulses are labeled G_P and G_R return pulses, respectively, and are used to initialise the *k*-space location identically for each spin-echo acquisition period.

follow a pattern of alternating polarity and decreasing amplitude (*1*, *19*). Given adequate dephasing strength, these spoiler gradients eliminate signal from unwanted coherence pathways. The read gradient channel includes N_{GE} lobes of alternating polarity for acquisition of N_{GE} gradient echoes during each spin-echo period (labeled G_R acq pulses in Fig. 1). Note that N_{GE} represents the factor by which image acquisition rate is increased. Following each read gradient lobe, a phase gradient blip (labeled G_P blip increment in Fig. 1) increments the *k*-space trajectory in a manner shown in Fig. 2. The resulting *k*-space trajectory for each echo is that of an interleaved segmented EPI acquisition (*20*). In order to ensure identical T_2^* weighting of each echo image, read and phase gradients were used, in conjunction with the RF refocusing pulses, to return the spins to the same initial *k*-space coordinate prior to each spin-echo acquisition period. (These gradient pulses are labeled in Figs. 1 and 2 as G_R and G_P return pulses.)

In order to allow time for diffusion weighting or multiple RATE acquisitions with interleaved echo times, variable delays during the first interecho period (TE_1) have been incorporated. These variable delays are situated at points of zero net spin dephasing to prevent the induction of variable diffusion weighting. Additionally, appropriate magnetization preparation (saturation-recovery, spin-locking, etc.) prior to the exci-

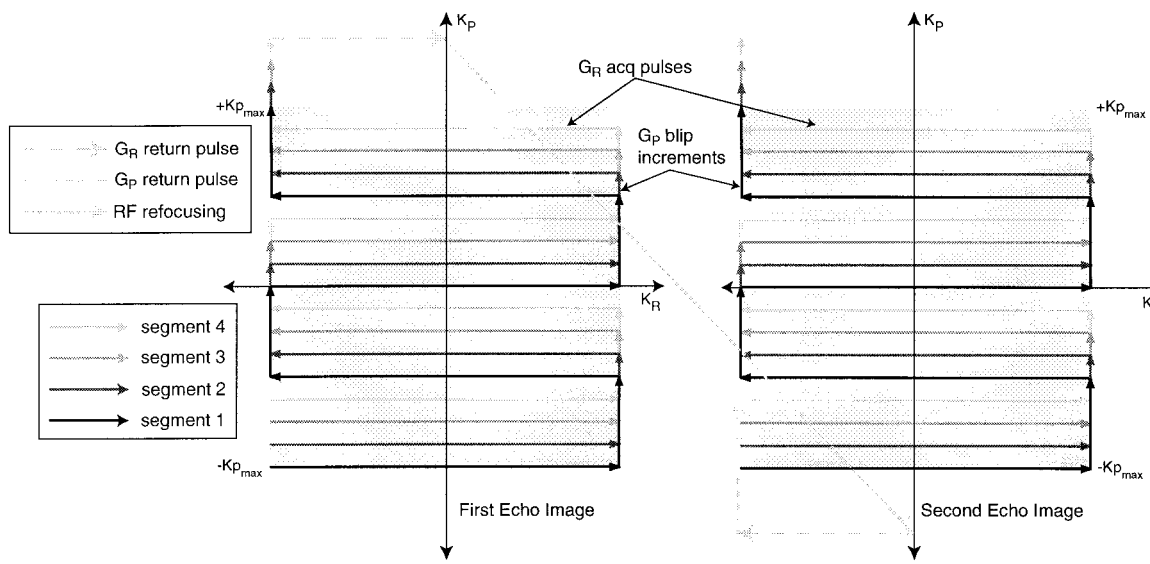

FIG. 2. An example of *k*-space trajectory for any two consecutive echo images of a RATE acquisition with $N_{GE} = 4$ and 16 total phase encode steps. The return pulses and RF refocusing pulse (see Fig. 1) are used to initialize *k*-space identically for each echo image. These pulses are shown here for the fourth of four segments only.

tation pulse can be implemented for correlation of various parameters with T_2.

Running a reference scan in the absence of phase-encoding gradients provides the necessary phase information required to reconstruct each echo image. Specifically, *k*-space data from both the reference and the image data are Fourier transformed in the read-encode direction. The phases of the reference scan data are then subtracted from the phases of the image data, and the resulting image data are Fourier transformed in the phase-encode direction to produce the image.

EXPERIMENTAL

^{1}H NMR experiments were performed at 85 MHz on a 31-cm-bore 2.0-T superconducting magnet equipped with Acustar actively shielded imaging gradients and operated with a Bruker Avance console. A 50-mm-diameter birdcage coil was used for RF transmission and signal reception. Excitation was achieved with a 2-ms-duration sinc pulse, refocusing with a 500-μs, 16-segment 5.4π composite pulse designed to be relatively insensitive to both B_0 and B_1 field variations (*21*), and unwanted magnetization was eliminated using an alternating and decreasing pattern of spoiler gradients (*1, 19*) with a minimum dephasing strength of 2π per pixel.

Data were collected from three cylindrical agar gel samples, 12 mm in diameter, with approximate agar concentrations of 2, 4, and 6% by weight. The field-of-view (FOV) was 50 mm, generated using 128 samples per echo (N_s) and 128 phase-encoding steps (N_p), and the number of echoes (NE) collected was 16. The total number of segments required was N_p/N_{GE}. Echo times (TE), number of echoes, receiver bandwidth (BW), number of averages (NA), and N_{GE} were varied.

In vivo data were collected from a 220-g, female Sprague–Dawley rat, which was ventilated via tracheotomy tube with a 40/60% oxygen/nitrogen gas mixture and anaesthetized with the inclusion of 1.2% halothane. To minimize motion artifacts the rat was paralyzed with a 0.05-mL ip injection of tubocurare. Blood pressure, pO_2, pCO_2, and temperature were observed and maintained in a normal physiological range for all measurements. Three multiecho image sets were collected, all of which used 35-mm FOV, 8 NE, 20-ms TE, 2-mm slice thickness, 3-s TR, 2 NA, and following different parameters: (i) 96 $\times$ 96 $N_S \times N_P$, 15.15-kHz BW, 1 N_{GE}, $\approx$9 1/2 min acquisition time (t_{acq}); (ii) 96 $\times$ 96 $N_S \times N_P$, 67-kHz BW, 8 N_{GE}, 72-s t_{acq}; (iii) 64 $\times$ 64 $N_S \times N_P$, 125 kHz BW, 16 N_{GE}, 24-s t_{acq}. From each of these image sets, single component T_2 values were computed on a pixel-by-pixel basis by fitting the log of the echo magnitudes to a linear function. Echo magnitudes with SNR < 6 were ignored to prevent bias from background noise.

To assess the ability to measure multiexponential T_2 using RATE, two further image sets were acquired, each with 32 NE, one with conventional acquisitions (1 N_{GE}), 40-kHz BW, and 12-ms TE, the other using RATE (4 N_{GE}), 100-kHz BW, 13.25-ms TE_1 and 14-ms TE. T_2 spectra were generated by fitting the 32 echo magnitudes to a series of 64 decaying exponential functions (*22*) with time constants ranging logarithmically from three quarters of the shortest echo time to three halves of the longest. The fitting also included a minimum energy constraint, which was adjusted to increase the $\chi 2$ statistic by 0.75% beyond that of the unconstrained fit (*23*).

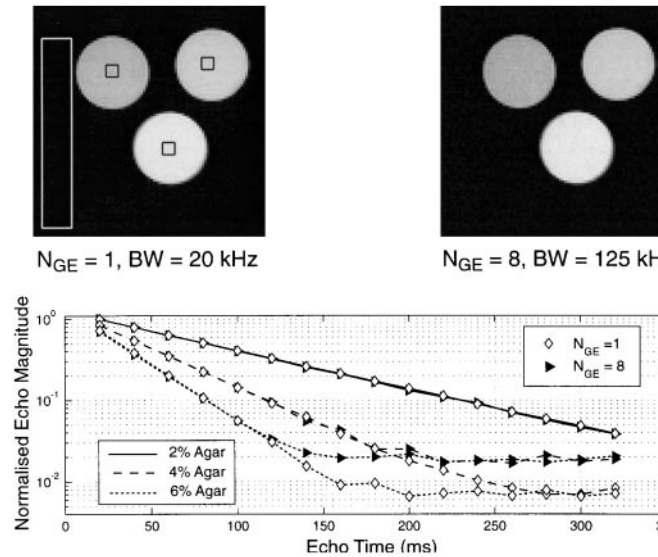

FIG. 3. Top: First echo images from a multiecho imaging sequence, one generated with a conventional acquisition ($N_{GE} = 1$) and the other with a RATE acquisition ($N_{GE} = 8$). Boxes define image and background ROIs, and images have been cropped to a 38 $\times$ 38 mm FOV. Bottom: Mean echo magnitudes of the image ROIs from conventional and RATE acquisitions. T_2 and SNR measurements from these data can be found in Table 1.

RESULTS AND DISCUSSION

Figure 3 shows the first echo images and respective multiecho decay curves from two image sets of the agar gels, one at low bandwidth (BW = 20 kHz) suitable only for conventional acquisitions (i.e., $N_{GE} = 1$), and one at high bandwidth (BW = 125 kHz) with $N_{GE} = 8$. For each of these images TE was 20 ms, which was near the minimum echo time attainable with $N_{GE} = 8$ and all other parameters constant. It is immediately apparent that the conventional and RATE decay curves are in excellent agreement, differing only in noise level. The background signal-to-noise ratio (SNR_B) was defined as mean image intensity of a region of interest from within the sample divided by the standard deviation of pixels from a background ROI—see Fig. 3. The ratio of mean to standard deviation of image intensity of data only from within the sample defined the image SNR (SNR_I). From within the image ROI, T_2s were calculated on a pixel-by-pixel basis and Table 1 summarizes observed SNRs and T_2s for a variety of imaging parameters. Not surprisingly, the SNR_B measurements are approximately proportional to $(NA/BW)^{1/2}$. Since the number of averaged acquisitions possible per unit time is proportional to N_{GE} it follows that the SNR_B per unit time is proportional to (N_{GE}/

TABLE 1
SNR and T_2 Measurements of Agar Gel Samples Data from Acquisition with 16 NE and Various BW, TE, NA, and N_{GE} Parameters

N_{GE}	BW (kHz)	TE (ms)	NA	$\approx t_{acq}$ (min)	SNR_B (in 2% agar)	SNR_I (in 2% agar)	2% agar T_2 (ms)	4% agar T_2 (ms)	6% agar T_2 (ms)
1	20	20	2	8 1/2	162	84	93 ± 2.0	46 ± 0.9	31 ± 1.3
1	125	20	2	8 1/2	67	44	92 ± 2.7	46 ± 2.0	32 ± 2.2
1	50	12	2	8 1/2	105[a]	78[a]	88 ± 2.2	43 ± 1.5	30 ± 1.4
2	125	12	2	4 1/4	62[a]	61[a]	89 ± 2.6	45 ± 2.1	31 ± 1.4
8	125	20	2	1	64	50	92 ± 3.4	45 ± 2.0	32 ± 1.6
8	125	20	8	4 1/4	133	83	92 ± 2.8	45 ± 1.6	31 ± 1.2
8	125	20	16	8 1/2	182	64	89 ± 2.2	43 ± 1.5	30 ± 1.4
16	125	32	2	1/2	62[b]	42[b]	92 ± 5.9	44 ± 3.5	31 ± 2.8

[a] Corrected by exp(−8 ms/92 ms) to compare with data collected at 20-ms TE.
[b] Corrected by exp(+12 ms/92 ms) to compare with data collected at 20-ms TE.

BW)$^{1/2}$. Given an otherwise fixed set of imaging parameters, the required bandwidth increases proportionally to the N_{GE}, making SNR_B per unit time approximately constant. The SNR_I, which is affected not only by thermal noise but also by systematic errors in the imaging sequence (e.g., ghosting), was found to be approximately the same for N_{GE} of 1, 2, 8, and 16 with a fixed BW.

Animal imaging data are presented in Figs. 4 and 5. Figure 4 shows the first echo image of the rat brain from the conventional acquisition for anatomical reference and three T_2 maps calculated from each of the three eight-echo image sets acquired. The T_2 estimates and variance were similar for all three imaging protocols, despite an 8-fold reduction in acquisition time at a fixed resolution (96 × 96) or a 24-fold reduction at a 50% reduced resolution (64 × 64). Increasing TE beyond 20 ms would allow further increased N_{GE} and thus further reduced acquisition times. Figure 5 shows the T_2 decay curves and corresponding T_2 spectra from a trigeminal nerve ROI, both of which show a close correspondence between the conventional and RATE data. The increased smoothness of the RATE data T_2-spectrum compared to that from the conventional acquisition is reflective of a lower SNR, but the mean component T_2s and signal fractions are quite similar (see legend to Fig. 5).

If simple single-component T_2 maps are desired, there are some alternative techniques to consider. Again, repeated EPI or segmented EPI can be used to rapidly generate T_2 maps. While this approach has the benefit of being easily implemented on many systems without pulse sequence development, it is gen-

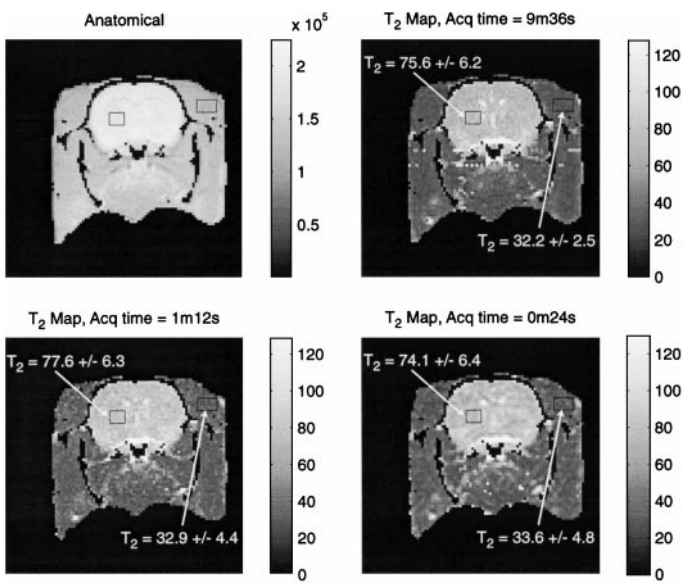

FIG. 4. Top: First echo image from a conventional multiecho acquisition and a corresponding T_2 map. Bottom: Similar T_2 maps derived acquisitions using N_{GE} of 8 and 24. Boxes identify gray matter and muscle ROIs and their mean ± standard deviation T_2.

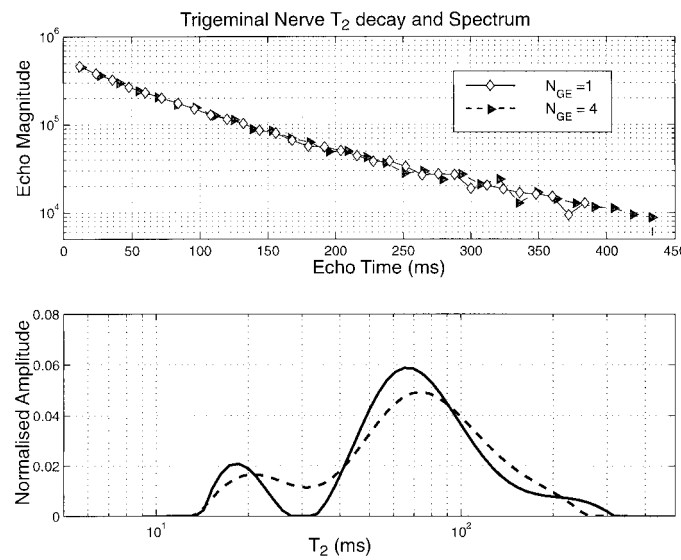

FIG. 5. Echo magnitudes of trigeminal nerve ROIs from conventional and RATE acquisitions (top) and their corresponding T_2 spectra (bottom). For the conventional acquisition, the two broad T_2 components have signal fractions and mean T_2s of 13% at 19 ms and 87% at 87 ms. For the RATE acquisition the components are 15% at 22 ms and 85% at 87 ms.

erally limited in spatial resolution and/or minimum acquisition/echo time compared with RATE, because of the inclusion of multiple echoes. Repeated SNAPSHOT FLASH images can be collected in rapid succession to generate a T_2 decay curve on the order of 30 s (*12*). This approach provides the ability to acquire at short echo times without increasing total acquisition time; however, the trade off is a reduced SNR resulting from the small-tip excitation pulses required. For comparison, Deichmann *et al.* (*12*) quote similar variance T_2 maps to the RATE data collected in approximately 30 s (Table 1), but their data were collected at 7 T in nearly 2 min. Their measurements, however, included echoes at TEs as short as 4 ms, which would not be attainable with RATE. A completely different approach, T_2-FARM (*13*), is inherently single shot, thereby allowing for much faster acquisitions to either RATE or SNAPSHOT FLASH, but at the expense of SNR and complex data processing. For comparison, similar or poorer variance T_2 maps to RATE data herein were presented from 3-s acquisitions at similar B_0 field (1.89 T), but from voxel sizes approximately 70 times that used in rat brain here.

On the other hand, if the objective is to measure a MET_2 decay curve using MRI, we are unaware of any other published techniques to which RATE can be compared. In principle, one could acquire repeated EPI or segmented EPI images while varying echo time, but this will require a much longer acquisition time when NE is large and will result in increased diffusion losses at long echo times. Thus, the efficacy of RATE for MET_2 quantification depends only on two issues: (i) whether adequate gradient characteristics (strength, switching time, and eddy currents) exist to implement the desired pulse sequence and (ii) whether SNR can be sacrificed for the sake of reduced acquisition times. Given a system that will satisfy the first condition, the tradeoff of SNR vs acquisition time is sample and experiment dependent. One scenario in which it may prove worthwhile is the integrated measurement of a given NMR parameter (e.g., T_1, $T_{1\rho}$, . . .) with T_2 through repeated CPMG acquisitions using variable preparations.

ACKNOWLEDGMENTS

The authors thank Terry Nixon, Peter Brown, and Scott MacIntyre for technical support. We also acknowledge financial support from NIH Grant NS34834.

REFERENCES

1. C. S. Poon and R. M. Henkelman, Practical T2 quantitation for clinical applications. *J. Magn. Reson. Imaging* **2**(5), 541–553, 1992.
2. A. MacKay, K. Whittall, J. Adler, D. Li, D. Paty, and D. Graeb, In vivo visualization of myelin water in brain by magnetic resonance. *Magn. Reson. Med.* **31**(6), 673–677, 1994.
3. M. D. Does and R. E. Snyder, T2 relaxation of peripheral nerve measured in vivo. *Magn. Reson. Imaging* **13**(4), 575–580, 1995.
4. P. J. Gareau, B. K. Rutt, C. V. Bowen, S. J. Karlik, and J. R. Mitchell, In vivo measurements of multi-component T2 relaxation behaviour in guinea pig brain. *Magn. Reson. Imaging* **17**(9), 1319–1325, 1999.
5. J. E. M. Snaar and H. Van As, A method for the simultaneous measurement of NMR spin–lattice and spin–spin relaxation times in compartmentalised systems. *J. Magn. Reson.* **99,** 139–148, 1992.
6. R. Harrison, M. J. Bronskill, and R. M. Henkelman, Magnetization transfer and T2 relaxation components in tissue. *Magn. Reson. Med.* **33**(4), 490–496, 1995.
7. M. D. Does, C. Beaulieu, P. S. Allen, and R. E. Snyder, Multi-component T1 relaxation and magnetisation transfer in peripheral nerve. *Magn. Reson. Imaging* **16**(9), 1033–1041, 1998.
8. G. J. Stanisz and R. M. Henkelman, Diffusional anisotropy of T2 components in bovine optic nerve. *Magn. Reson. Med.* **40**(3), 405–410, 1998.
9. S. Peled, D. G. Cory, S. A. Raymond, D. A. Kirschner, and F. A. Jolesz, Water diffusion, T(2), and compartmentation in frog sciatic nerve. *Magn. Reson. Med.* **42**(5), 911–918, 1999.
10. G. J. Stanisz, A. Kecojevic, M. J. Bronskill, and R. M. Henkelman, Characterizing white matter with magnetization transfer and T(2). *Magn. Reson. Med.* **42**(6), 1128–1136, 1999.
11. M. D. Does and J. C. Gore, Compartmental study of diffusion and relaxation measured in vivo in normal and ischaemic rat brain and trigeminal nerve. *Magn. Reson. Med.* **43**(6), 837–844, 2000.
12. R. Deichmann, H. Adolf, U. Noth, S. Morrissey, C. Schwarzbauer, and A. Haase, Fast T2-mapping with snapshot flash imaging. *Magn. Reson. Imaging* **13**(4), 633–639, 1995.
13. C. A. McKenzie, Z. Chen, D. J. Drost, and F. S. Prato, Fast acquisition of quantitative T2 maps. *Magn. Reson. Med.* **41**(1), 208–212, 1999.
14. D. A. Yablonskiy, Quantitative T2 contrast with gradient echoes. Proceedings of the International Society of Magnetic Resonance in Medicine, p. 431, 8th Meeting, Denver, 2000.
15. S. J. Graham and M. J. Bronskill, MR measurement of relative water content and multicomponent T2 relaxation in human breast. *Magn. Reson. Med.* **35**(5), 706–715, 1996.
16. G. Saab, R. T. Thompson, and G. D. Marsh, Multicomponent T2 relaxation of in vivo skeletal muscle. *Magn. Reson. Med.* **42**(1), 150–157, 1999.
17. C. S. Landis, X. Li, F. W. Telang, P. E. Molina, I. Palyka, G. Vetek, and C. S. Springer, Jr., Equilibrium transcytolemmal water-exchange kinetics in skeletal muscle in vivo. *Magn. Reson. Med.* **42**(3), 467–478, 1999.
18. D. Tyler, L. Marciani, and P. Gowland, Accurate imaging measurement of T2 from a single echo train. p. 432, Proceedings of the International Society of Magnetic Resonance in Medicine, 8th Meeting, Denver, 2000.
19. A. P. Crawley and R. M. Henkelman, Errors in T2 estimation using multislice multiple-echo imaging. *Magn. Reson. Med.* **4**(1), 34–47, 1987.
20. G. C. McKinnon, Ultrafast interleaved gradient-echo-planar imaging on a standard scanner. *Magn. Reson. Med.* **30,** 609–616, 1993.
21. C. S. Poon and R. M. Henkelman, 180° refocussing pulses which are insensitive to static and radiofrequency field inhomogeniety. *J. Magn. Reson.* **99,** 45, 1993.
22. K. P. Whittall and A. L. MacKay, Quantitative interpretation of NMR relaxation data. *J. Magn. Reson.* **84**(1), 134–152, 1989.
23. S. J. Graham, P. L. Stanchev, and M. J. Bronskill, Criteria for analysis of multicomponent tissue T2 relaxation data. *Magn. Reson. Med.* **35**(3), 370–378, 1996.